TITLE:

Mcam stabilizes a luminal progenitor-like breast cancer cell state via Ck2 control and Src/Akt/Stat3 attenuation

AUTHORS AND AFFILIATIONS:
Ozlen Balcioglu[1,2], Brooke L. Gates[1,2], David W. Freeman[1,2], Berhane M. Hagos[3], Elnaz Mirzaei Mehrabad[4], David Ayala-Talavera[1,2] and Benjamin T. Spike[1,2,4]

[1]Huntsman Cancer Institute, University of Utah, Salt Lake City, UT 84112 USA
[2]Department of Oncological Sciences, University of Utah, Salt Lake City, UT 84112 USA
[3]Current Address: Emergency Medicine, Oregon Health & Science University School of Medicine, Portland, OR 97239 USA
[4]School of Computing, University of Utah, Salt Lake City, UT 84112 USA

Corresponding Author: Benjamin T. Spike
Corresponding Author Email: Benjamin.Spike@hci.utah.edu

KEYWORDS: MCAM, Breast Cancer, Cell State, Plasticity

CONFLICT OF INTEREST STATEMENT:
The authors declare no conflict of interest exists.

Running title: Mcam promotes a plastic mammary luminal progenitor state

ABSTRACT:

Breast cancers are categorized into subtypes with distinctive therapeutic vulnerabilities based on expression of clinically targetable receptors and other genes that mimic cell types of the normal gland. Here, we tested the role of the plasma membrane-integral glycoprotein Mcam in breast cancer cell state control and tumorigenicity using a murine tumor cell line (Py230), that exhibits lineage and tumor subtype plasticity. Mcam knockdown (KD) Py230 cells exhibit increased mesenchymal morphology, migration, Src/Fak/Mapk/Paxillin adhesion complex signaling and Pi3K/Akt, Stat3 and Stat5a activation. They also show a transcriptional switch from a hormone-sensing/luminal progenitor state toward alveolar and basal cell states. Reminiscent of archival human breast cancers and patient derived organoid expression data associated with endocrine resistant disease, Mcam KD Py230 cells were refractory to growth inhibition by tamoxifen *in vitro*. Endocrine resistance and cell state change resulting from Mcam KD were reversed by inhibition of Stat3 or the upstream activating kinase Ck2. Finally, while Mcam KD cells exhibited more aggressive phenotypes *in vitro*, they showed reduced tumorigenicity and lacked Sox10+/neural crest cell state acquisition *in vivo*. Our studies uncover breast cancer

cell state plasticity dependent on Mcam, Ck2, and Stat3 with implications for progression, evasion of targeted therapies and combination therapy design.

INTRODUCTION

Breast cancers exhibit cellular and subtype heterogeneity that complicates treatment and contributes to disease progression. Whereas hormone receptor (estrogen and progesterone) positive (HR+) and Her2 amplified (Her2+) cancers are treated with molecular therapies targeting these molecular drivers, triple negative breast cancers (TNBC) lack these molecular targets (1). Transcriptional profiling has identified intrinsic breast cancer subtypes that partially overlap with these clinical subtype designations and with cellular compartments of the normal breast (2). For instance, Luminal A and B subtypes are typically HR+, the 'Her2-enriched' intrinsic subtype comprises most Her2+ tumors, and the Basal-like breast cancer designation encompasses most TNBCs.

The origins of this heterogeneity remain controversial, and the molecular mediators are incompletely understood. However, it is generally held that tumor subtype reflects particular combinations of driver mutations and intrinsic characteristics of the cell of origin (1,3,4). Consistent with this, experiments in mice that target drivers to different normal compartments of the mammary give rise to different subtypes of breast cancer (5,6). However, cell plasticity has also emerged as a significant contributor to intra- and inter-tumoral heterogeneity and likely plays an important role in therapy resistance, dormancy, and metastasis (7,8). A classic example of plasticity in cancer progression involves epithelial to mesenchymal transitions (EMT) which is heavily implicated in tumor cell migration, invasion, and dissemination to form deadly metastases in breast and other epithelial tissues (6,9,10). Furthermore, lineage plasticity leading to subtype switching in breast cancer progression is now well documented (11). Thus, in another example, hormone dependent tissues often give rise to hormone dependent cancers, but these can sometimes transition into hormone-independent phenotypes, thus evading conventional hormone-blocking therapy. In breast cancer, this conversion has been associated with activation of EMT or alternatively a state transition to a hormone insensitive, alveolar progenitor program. Alveolar programs are classically driven by dedicated transcription factors such as Elf5, Stat3 or Stat5 (12-14). Identifying and understanding the upstream molecular regulators of such lineage plasticity in breast and other cancers could reveal valuable therapeutic vulnerabilities.

In this study, we chose to examine a potential role for the membrane-integral cell-surface glycoprotein MCAM (CD146; MUC18; S-Endo-1; and Gicerin) in regulating breast cancer cell state plasticity based on several prior observations. First, our prior studies showed that Mcam is broadly expressed in multipotent fetal mammary stem cells (15). Mcam is also an established marker of pericytes noted for their high intrinsic cellular plasticity, although lower-level expression in a variety of other cells and tissues, including multipotent mammary stem cell compartments, has been reported (16-18). MCAM is upregulated in a variety of cancers and has different activities depending on the target cancer/cell type (16,19). In breast cancer, elevated expression of MCAM has been associated with basal-like cancer and poor prognosis (16,20). Experimental overexpression of MCAM in MCF7 and SKBR-3 cells (HR+ and HER2+ cell lines, respectively) drives EMT and promotes tumorigenesis in xenograft settings (21). However, MCAM has also been reported to be tumor suppressive in some cancer settings and recent work has challenged the notion that it is universally or even widely oncogenic (22,23).

Mechanistically, MCAM has been implicated in a variety of biological processes relevant to mammary cell identity, development and cancer. MCAM has been reported to mediate cell-cell interactions between heterotypic cells during extravasation of immune and tumor cells (16). It may bind S100A7/8/9, which plays a key role in cell motility on neighboring cells and can bind extracellular matrix laminin-α4 *in vitro*, controls integrin-β1 levels (24,25). Inside the cell, MCAM regulates integrin mediated signaling (through FAK regulation and ERM binding), Wnt-mediated planar cell polarity, and has been reported to possess Ck2, Pka and Pkc binding/phosphorylation motifs (16,26,27). Yet, how Mcam integrates outside-in signaling with cell state across different types of breast cancer and the relevant signaling cascade(s) remain to be determined, particularly in luminal breast cancer cells where it has thus far been studied principally through acquired or experiment overexpression (21).

We show Mcam is a potent regulator of cell state plasticity in Py230 cells, a luminal progenitor/stem cell-like mammary tumor cell line derived from the MMTV-PyMT mouse model. In contrast to prior studies where MCAM overexpression drove EMT and the associated loss of luminal epithelial characteristics in mammary cells, we show that Mcam knockdown (KD) in Py230 cells alters signaling through multiple adhesion and growth factor related signaling cascades leading to elevated Stat3 activity and a lineage switch away from hormone-sensing luminal progenitor state toward alveolar- and basal-like phenotypes with associated loss of

tamoxifen sensitivity *in vitro*. These changes were associated with altered activity of the master casein kinase II (Ck2) against multiple substrates and inhibition of Ck2 or Stat3 reversed the transcriptional state change elicited by Mcam KD. Alterations in cell state were also evident in transplanted tumors and included loss of transdifferentiation potential toward Sox10-positive neural crest phenotypes that have been previously associated with Py230 tumor aggressiveness (28). These results inform the development of combination breast cancer therapies that incorporate MCAM and/or CK2 and STAT inhibitors and point both to opportunities and potential challenges in clinical management of breast cancer.

RESULTS

Mcam blocks mesenchymal phenotypes in a murine luminal progenitor-like mammary cancer cell line.

MCAM expression has previously been associated with mesenchymal cells and phenotypes, including multipotent stromal cells, apical-basal epithelial polarity and EMT in cancers including breast cancer (19,22,29). However, we found that MCAM was detectable across diverse murine breast cancer cell lines including several designated as luminal and luminal progenitor-like (**Figure 1A,B**). We focused our attention on the Py230 cell line, a luminal progenitor/mammary stem cell-like line derived from MMTV-PyMT C57BL/6 mice, due to its luminal progenitor designation and high endogenous level of Mcam (**Figure 1A,B**) (6,28). We reduced total and surface Mcam levels in Py230 cells by transient transfection with a panel of Mcam directed siRNAs (**Supplementary Fig. 1A,B**) or by transducing cells with lentiviral vectors bearing a distinct Mcam-directed shRNA constructs (**Figure 1C,F, Supplementary Fig. S1D,E**). Although transfection efficiency and KD were modest in transient transfections (**Supplementary Fig. S1A,B**), we noted qualitative differences in cellular morphology and adhesion in a subset of cells in siMcam cultures as well as elevated expression of the focal adhesion associated protein, Paxillin (**Supplemental Fig. S1C**). Using stable, lentiviral-transduced, GFP-sorted Mcam knockdown (Mcam-KD) and control vector bearing Py230 cells, we obtained more robust Mcam KD and again observed consistent paxillin overexpression across three independently derived clones (**Figure 1C,F, Supplemental Fig. S1D-F**). Surprisingly, given Mcam's reported roles in promoting mesenchymal phenotypes, stable Mcam KD in Py230 cells increased mesenchymal features including elongated spindleoid morphology (similar to what we observed in transient transfections) and enhanced migration in scratch wound

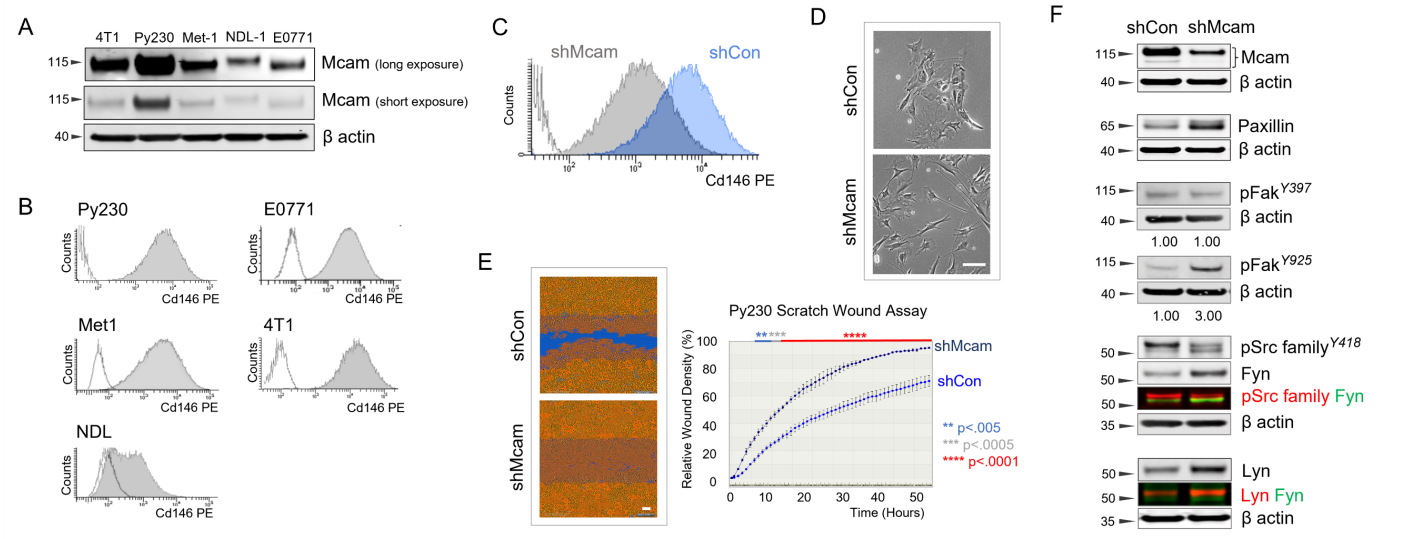

Figure 1. Cellular and molecular signaling changes following Mcam KD in Py230 cells. A) Western blot of mouse breast cancer cell lines. B) Flow cytometric analysis of cell surface Mcam expression across multiple murine mammary cancer cell lines. Unshaded histograms indicate unstained controls. C) Reduced surface Mcam levels in flow cytometric analysis of Mcam-KD Py230 cells. Unshaded histogram = unstained control cells. B) Mcam-KD does not change Py230 proliferation rate (IncuCyte) or C) survival in flow cytometric analysis. D) Phase contrast image of low density Mcam-KD Py230 cells showing a more elongated spindeloid appearance than controls. Scale bar = 100μm. E) IncuCyte scratch wound assay indicates Mcam-KD increases migration of Py230 cells. Scale bar = 100μm. Two-way ANOVA with Sidak's multiple comparisons test between shCon and shMcam. ns = not significant, *p<0.05, **p<0.01, ***p<0.001, ****p<0.0001. F) Western blot analysis of Mcam and altered focal adhesion related signaling in Mcam-KD Py230 cells and scrambled controls.

assays relative to scrambled shRNA controls (**Figure 1D,E**). These phenotypic changes were reproducible across multiple independently derived Mcam-KD Py230 clones, indicating that they are more likely to derive from alterations in Mcam levels than stochastic selection-based effects. Correlated with these phenotypes, we find that Mcam-KD Py230 cells elicit altered expression and activation of several focal adhesion-related signaling molecules including Paxillin, Fak, Src family, Fyn, and Lyn (**Figure 1F**) (30). These data indicate that in contrast to studies where Mcam expression or overexpression drives mesenchymal phenotypes in epithelial cells, Mcam reduction can also promote this effect. Mcam KD was inconsequential for overall proliferation and survival of Py230 cells in culture (**Supplemental Fig. S1G,H**).

Mcam controls cell state in Py230 cells.

Confluent cultures of Mcam-KD Py230 exhibited morphological heterogeneity that is distinct from confluent control cultures, suggestive of an altered cellular differentiation state (**Figure 2A**). Examination of the lineage related keratins, Krt14 (Basal) and Krt8 (Luminal), revealed a marked reduction in the frequency of uncommitted Krt8/14 co-expressing cells upon Mcam KD (**Figure 2B**). To further characterize cell state

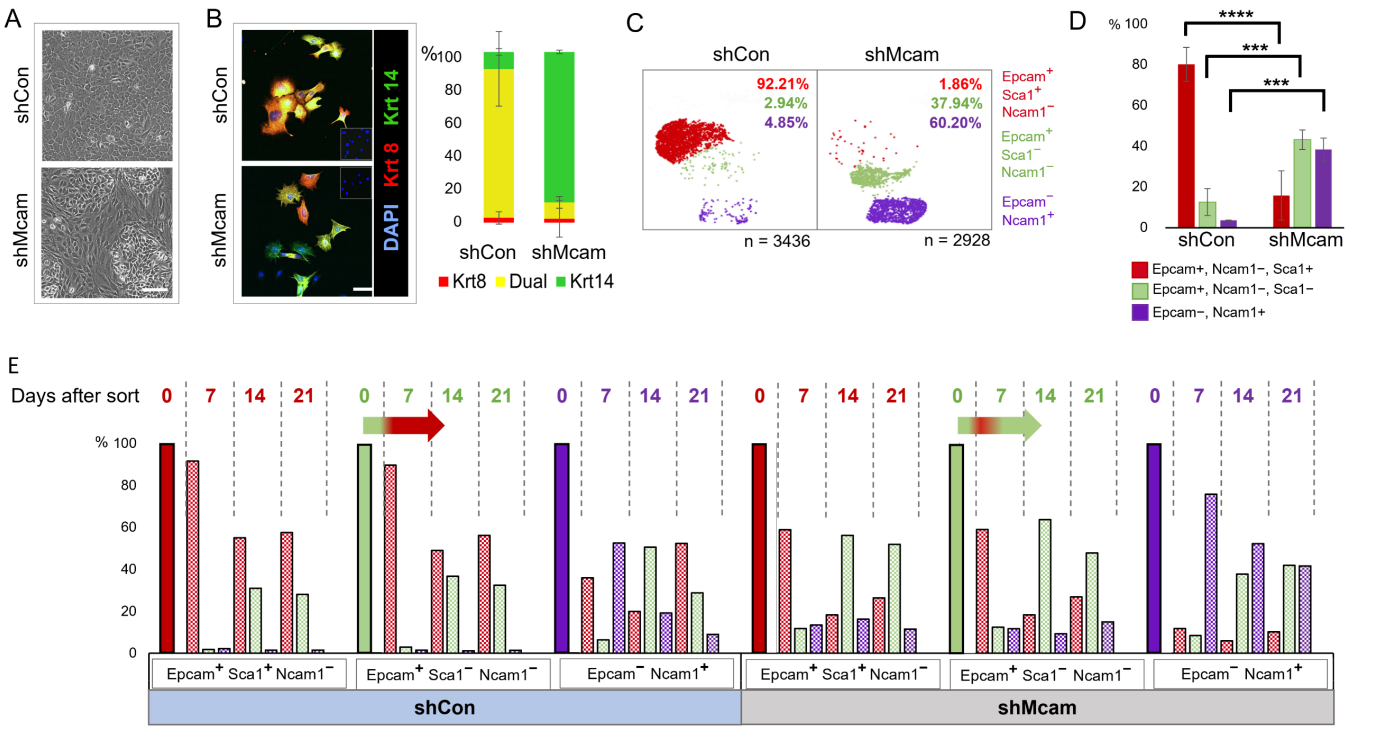

Figure 2. Cell-state change following Mcam-KD in Py230 cells. A) Phase contrast image of confluent Mcam-KD and control Py230 cultures. Scale bar = 100µm. B) Altered expression of lineage associated Krt8 (red) and Krt14 (green) in Py230 Mcam-KD cultures. Scale bar = 100µm C) scRNA-seq profiles from control and Mcam-KD cells reveal three major subpopulations that are identifiable by expression of previously described mammary lineage markers (31) . D) Bar graph of flow cytometric analysis in triplicates confirms proportional skewing among cells expressing these three marker proteins that mirrored subpopulations identified by scRNA-seq (n=3 independent clones per genotype). Error bars = SD. Two-way ANOVA with Tukey multiple comparison test: ns = not significant, *p<0.05, **p<0.01, ***p<0.001, ***p<0.0001. E) Interconversion of Py230 subpopulations upon FACS separation and culture for 0, 7, 14 or 21 days. Horizontal arrows show immediate conversion of Epcam+Sca-Ncam- cells to Sca+ within one week followed by reversion in to Sca- predominance in Mcam-KD cells by week 2.

changes resulting from Mcam KD, we sequenced transcriptomes from thousands of single control and Mcam-KD Py230 cells (**Figure 2C**). UMAP graphical representation of the data revealed three major transcriptional cell states with differential representation between control and Mcam-KD cells (**Figure 2C, Supplementary Fig. S2A,B**). Control transcriptional profiles principally occupied a continuous graphical space at the upper left of the graph with a minority of cells in the other regions, whereas Mcam-KD cells exhibited a greater proportion of cells in these latter graphical regions with only a minority of cells in the region of the graph occupied by the main group of control cells (**Figure 2C**). Surveying the levels of previously described markers of distinct mammary cell states, we observed that transcript levels for Epcam and Sca1, delineate the major transcriptional states identified in the UMAPs as Epcam+Sca1^{High}, Epcam+Sca1^{Low} and Epcam-Sca1^{High} (31). We further determined that the Epcam- cells express Ncam1 whereas Epcam+ cells do not (**Figure 2C**). Flow cytometric analysis of surface protein expression confirmed population skewing that mirrored scRNA-seq (**Figure 2D, Supplementary Fig. S2C,D**). Flow cytometry and scRNA-seq of additional independent clones

demonstrated consistent loss of the Epcam+Sca1^{High} cell state when Mcam was knocked down although some variance in the final population frequencies was observed (**Supplementary Fig. S2B-D**). To ensure these effects result from Mcam KD specifically, we utilized a shRNA resistant Mcam overexpression (Mcam OE) vector to re-express Mcam in our Py230 Mcam-KD cells. Mcam re-expression restored predominance of the Epcam+Sca1^{High} profile while Epcam+Sca1^{low} and Epcam-Ncam+ cell populations were restored to near baseline proportions (**Supplementary Fig. S2E-H**). We also determined that all three populations were able to reestablish distributions observed in their respective parent populations within 3 weeks of cell sorting, although kinetics for redistribution from the Epcam-Ncam+ of each genotype were slower than other populations (**Figure 2E**). Critically, while sorted Epcam+Sca1^{Low} cells of both genotypes rapidly (within one week) generated Epcam+Sca1^{High} cells, the Epcam+Sca1^{High} cell type was rapidly (within two weeks) depleted in Mcam-KD cells (**Figure 2E**). Thus, Mcam-KD alters cell state distributions in Py230 by destabilizing the Epcam+Sca1^{High} phenotype.

Mcam attenuates Casein Kinase 2 and Stat3/5 activity in Py230 cells to stabilize a hormone-sensing, luminal progenitor state.

Epcam and Sca1 have previously been proposed to distinguish alveolar progenitors (AP) from hormone sensing luminal progenitors (HSP/LP) (31). We took a comparative transcriptomics approach to determine whether Py230 transcriptomes mimic these progenitor states more broadly. Py230 cells shared significant expression similarity with HSP/LP transcriptional states while the majority of Mcam-KD Py230 cells resembled AP and basal cell states of the normal gland (**Figure 3A-C, Supplementary Fig. S3A**) (15,32). We also performed gene set enrichment analysis (GSEA) of adult murine mammary gland luminal progenitor-, luminal-, alveolar-, and basal-related programs to confirm subtype classification (**Figure 3B, Supplementary Fig. S3A**) (15,33). Although we noted upregulation of neural crest associated genes in Mcam-KD Py230 cells, we determined that several of these genes are also expressed in normal mammary alveolar and basal cell types and do not necessarily indicate loss of mammary specification (**Figure 3C, Supplementary Fig. S3A**) (15).

In order to identify underlying regulatory programs that contribute to MCAM mediated cell state control, we examined enriched categories within the differentially expressed gene signatures between control cells and Mcam-KD Py230 cells using EnrichR (34). Genes upregulated in Mcam-KD cells were significantly enriched for

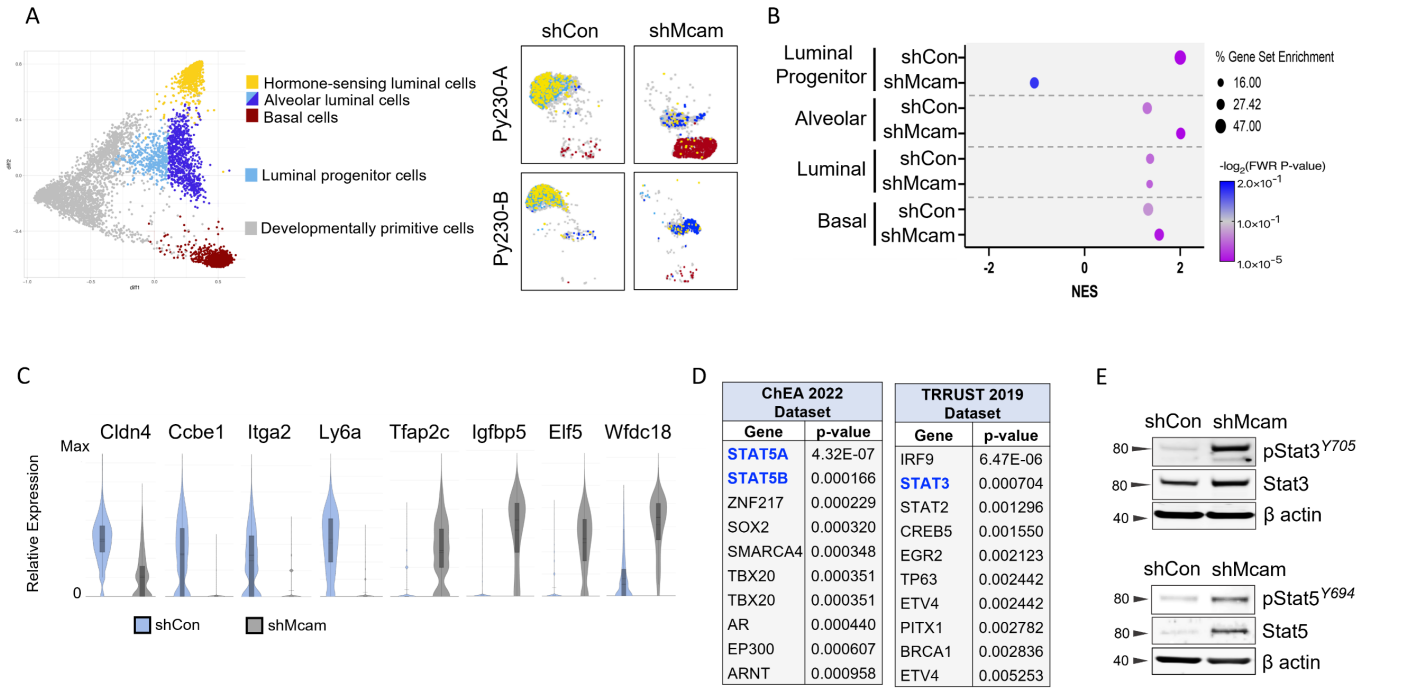

Figure 3. MCAM expression is associated with a mammary luminal progenitor phenotype. A)The top and bottom five differentially expressed genes between the adult mammary cell types identified in the diffusion map from Giraddi et al. (left) (ref. 15), identify different cell states in Py230 control and Mcam-KD cells (right). B) Bubble plot generated from GSEA showing enrichment of shCon and shMcam for luminal progenitor and alveolar cell states respectively compared to normal mouse mammary cell populations from Giraddi et al. (15). C) Violin plots for relative expression of luminal and alveolar cell state markers in Py230 control (blue) and Mcam-KD (grey) cells. D) Top genes associated with shMcam Py230 cells from Enrichr analysis using ChEA and TRRUST datasets. E) Overexpressed and phosphorylated Stat3 and Stat5 in Py230-A cells.

target genes of the Signal Transducer and Activator of Transcription (STAT) family of transcription factors, consistent with the established role of STATs in regulating alveologenesis in the normal mammary gland (**Figure 3D**) (13,14,35). For instance, Tfap2c, Igfbp5, and Wfdc18 alveolar markers are known Stat3 targets and were upregulated in Mcam-KD cells (**Figure 3C**) (36-38). Elf5, a classic alveolar lineage specifier, was also upregulated in Mcam-KD cells (**Figure 3C**) (12). We examined Stat3 and Stat5A levels and activation in Py230 cells as these factors are strongly implicated in alveolar cell state control in the normal gland and have well documented roles in breast and other cancers (**Figure 3E, Supplementary Fig. S3B-D**) (14,39,40). Total Stat3 and 5A were modestly upregulated in Mcam-KD Py230 but based on their phosphorylation status these factors were strongly overactivated providing a mechanistic basis for the alveolar cell state adopted by Mcam-KD cells (**Figure 3E**).

To determine whether hyper-activation of Stats was required for the HSP/LP → AP switch, we treated Py230 cells with Stattic, a selective STAT3 inhibitor. Additionally, we looked at the effects of inhibitors of upstream regulators of Stat signaling including Ag490, an inhibitor of Jak2, and CX-4935 and GO289, casein

kinase 2 (Ck2) inhibitors (**Figure 4A-E, G, Supplementary Fig. S4B-E**) (35,41,42). We also tested the ability of the casein kinase 2 (Ck2) inhibitor, CX-4945 to block Stat hyperactivation and alveolar cell state transition in Py230 (**Figure 4A-C,G, Supplementary Fig. S4E**).

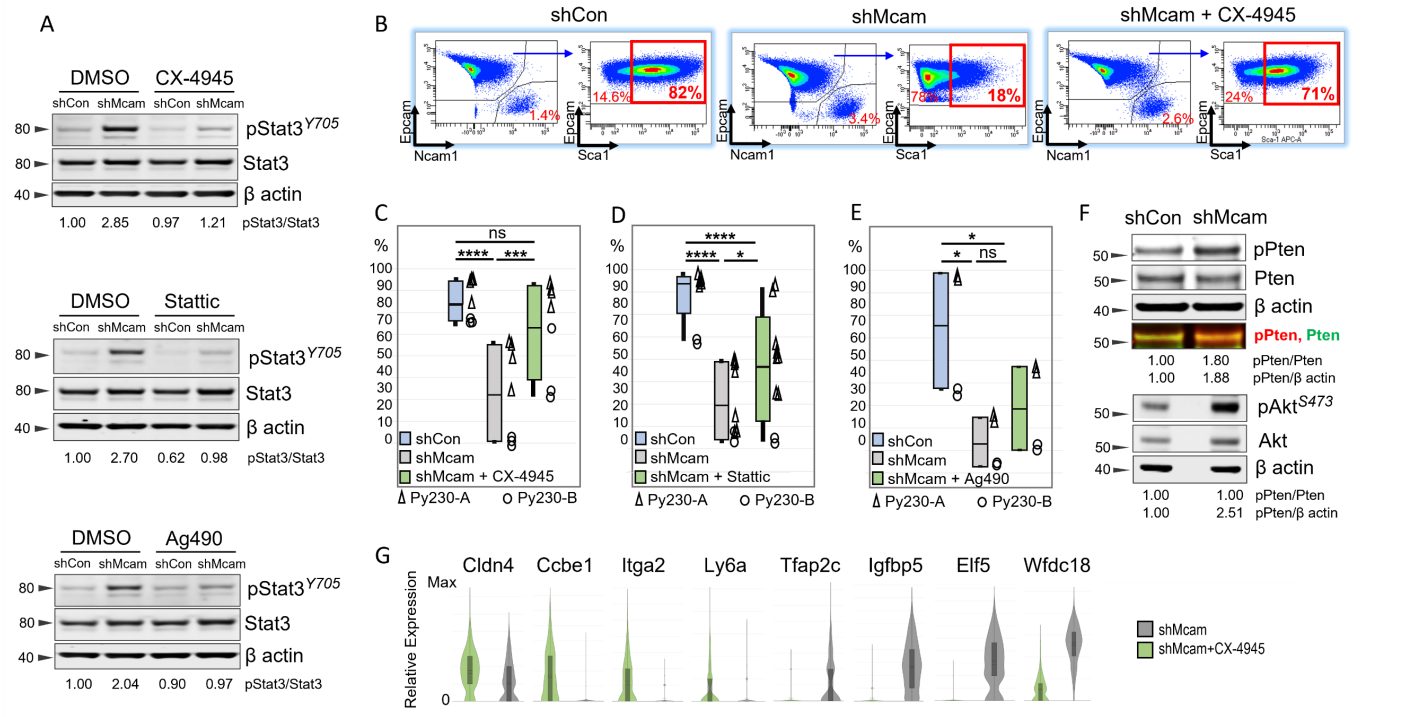

Figure 4. Overactive CK2 in Py230 shMcam cells maintains the alveolar progenitor phenotype. A) Over-expressed and phosphorylated Stat3 in Py230-A cells and its inhibition by the kinase inhibitors, CX-4945 10μM, Ag490 50μM, Stattic 1μM for 30 minutes in WB analysis. B) Representative FACS analysis of Py230-B cells treated with CX-4945 10μM for 7 Days and stained for Epcam, Sca1 and Ncam1. C-E) Graphs of FACS analysis showing the rescue of Epcam+, Sca1+ subpopulation frequencies in Py230-A and Py230-B cells treated with CX-4945 10μM for 7 Days C), with Stattic 1μM for 7 days D), and with Ag490 30μM for 7 days E). RM one-way ANOVA (Geisser-Greenhouse correction) with Tukey multiple comparison test: *p<0.05, **p<0.01, ***p<0.001, ****p<0.0001. F) Western blot analysis in Py230-A cells showing higher basal levels of pPten (Ser380/Thr382/383) and pAKT in Mcam-KD Py230. G) Gene expression in Py230-A cells treated with CX-4945 10μM for 7 Days (scRNA-seq).

Levels of pStat3 in Py230 Mcam-KD cells were decreased to near baseline levels by inhibition of Stats with Stattic or by inhibition of either upstream kinase (**Figure 4A**). Dramatically, the cell state skewing associated with Mcam-KD was also reversed by CX-4945, and to a lesser degree by Stattic whereas effects of Ag490 were not significant with respect to restoration of Epcam+Sca1^{High} LP-like cell state predominance (**Figure 4B-E, Supplementary Fig. S4B,C**). The role of Ck2 in Mcam-KD phenotypes was intriguing as Ck2 has not previously been implicated as a functional downstream target of MCAM in breast cells, although it has previously been implicated in breast tumorigenesis and cell state control of mammary cells (43). In previous studies, reduction of Ck2 levels in the colorectal cancer cell line, LoVo, led to reduced E-cadherin and other signs of EMT (44). However, in our study, Ck2 levels were unaffected by Mcam-KD and Ck2 inhibition did not

decrease E-cadherin or promote other EMT features (**Supplementary Fig. S4E,F**), rather we noted Mcam-KD was associated with augmented Ck2 activity toward Stat3 and phosphorylation of Phosphatase and Tensin homologue (Pten) at Ck2 specific sites Ser380/Thr382/Thr383 that promote its degradation and consequent hyperactivation of Akt (**Figure 4F, Supplementary Fig. S4G**) (44,45). The ability of CX-4945 to reverse these effects of Mcam-KD was also evident in single cell transcriptomic analysis. For instance, when we compare luminal and alveolar cell state markers across CX-4945 treated Mcam-KD cells, there was a restoration in the relative expression of luminal markers and a depletion of alveolar markers, suggesting a restoration of the luminal progenitor cell state (**Figure 4G, Supplementary Fig. S4H**). These data indicate that Mcam controls cell state in Py230 cells in a manner dependent on Ck2 and Stat3.

MCAM loss hallmarks aggressive luminal tumors.

Cell state transition is emerging as a key determinant of tumor heterogeneity and therapy evasion (6,7)(8,11). Considering the MCAM expression in luminal tumor cell lines and the HSP/LP/AP cell state transitions we observed in Mcam-KD Py230 cells above, we re-evaluated MCAM expression in breast cancers using publicly available breast cancer RNA-sequencing data from The Cancer Genome Atlas (TCGA) and across a recently published panel of patient-derived breast cancer models (PDM) (46,47). While we confirmed that elevated MCAM levels correlated with poorer prognosis in Basal and Her2 cell types, the reverse was true in a subset of Luminal cell types when examining patients treated with chemotherapy (**Figure 5A**). Chemotherapy treated Luminal cancers would tend to reflect a more aggressive subset than tumors treated with endocrine therapy as an adjuvant monotherapy. Examining MCAM expression across the various breast cancer subtypes, we found that MCAM was more highly expressed in Basal and Her2+ tumors than in Luminal tumors as previously reported (20) (**Figure 5B and Supplementary Fig. S5A**). However, we found that MCAM expression was generally reduced across all breast cancer subtypes relative to normal samples, with Luminal B tumors averaging lower levels than other tumor types (**Figure 5B**). It should be noted that to some extent MCAM expression levels in TCGA may also reflect different levels of stromal involvement since some stromal cells express high levels of MCAM. The Luminal B intrinsic subtype is distinguishable from Luminal A tumors by their poorer prognosis, more frequent endocrine resistance, greater proliferation, and associated increased expression of cell cycle progression related transcripts (1,3). However, underlying mechanisms that give rise to

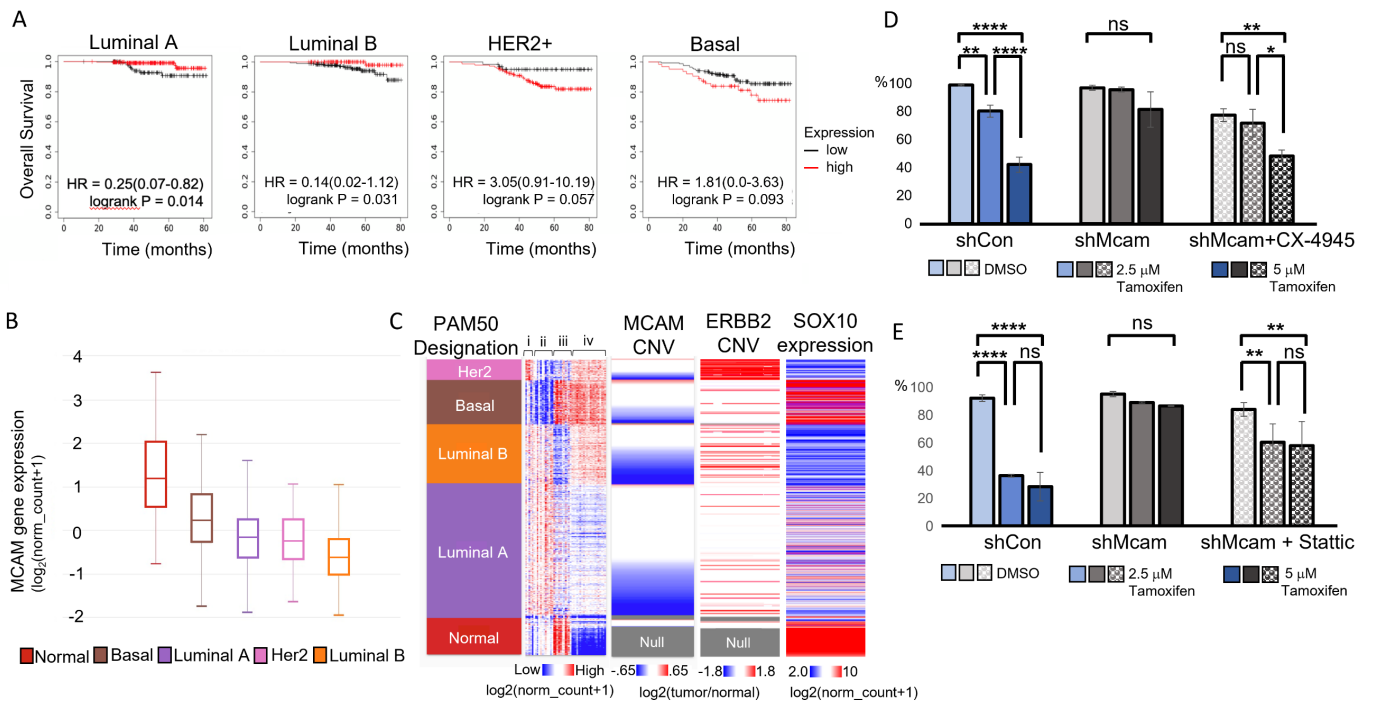

Figure 5. MCAM loss marks aggressive luminal tumors. A) Kaplan-Meier analysis of TCGA data breast cancer data, stratifying patients receiving chemotherapy between high and low MCAM expression. B) Box and whisker blot for MCAM expression across breast cancer subtypes in TCGA data. One-way ANOVA analysis, p<.0001 (f = 105.9), n=1247. C) TCGA breast cancer data organized by PAM50 designation, expression of PAM50 gene set, MCAM copy number variation, ERBB2 copy number variation, and SOX10 expression. The PAM 50 gene set can be broken down roughly into groups of genes related to ERBB2 expression (i), luminal genes including hormone receptor expression (ii), basal genes (iii), and proliferation genes (iv). D-E) IncuCyte proliferation assays of Py230 control and Mcam-KD cells with tamoxifen treatment shows that pretreatment with CX-4945 10μM for 7 days D) and pretreatment with Stattic 1μM for 7 days. E) rescue the tamoxifen sensitivity in Mcam-KD cells. One-Way ANOVA with Tukey Kramer Multiple Comparisons. ** p<0.05, ** p<0.01, *** p<0.001, **** p<0.0001*

these distinctions remain unclear. We noted that MCAM loss at the gene level was a surprisingly frequent event in breast cancer, especially in luminal tumors, with 43% of Luminal A and 63% of Luminal B type tumors showing reduced MCAM copy number (**Figure 5C, Supplementary Fig. S5B**). In the Luminal A subtype MCAM loss was associated with a trend toward increased expression of proliferation associated PAM50 genes and therefore a trend toward a more Luminal B like phenotype, likely due to concomitant amplification of Cyclin D1 at 11q (**Figure 5C, Supplementary Fig. S5B**) (4,48,49). To further validate these associations, we assessed MCAM expression across a compendium of PDMs (46). In agreement with our TCGA analysis, MCAM was most highly expressed in triple negative and HER2-amplified PDMs, with low but detectable expression across HR+HER2- models (**Supplementary Fig. S5A,D**). Interestingly, a significant proportion of PDM models (37.7%) are “triple positive”, expressing both HR receptors and ERBB2 (**Supplementary Fig. S5D**). Among these models many showed a reduced/absent Mcam even relative to other HR+ models, but two of these triple positive breast cancer (TPBC) models showed MCAM expression that was reduced when they

formed estrogen-independent (EI) outgrowths in mice (**Supplementary Fig. S5D, asterisks**) (46). We also noted a correlation between MCAM copy number reduction and TPBC status in archival TCGA data (**Figure 5C**), further supporting a relationship between MCAM loss, triple positivity, and aggressiveness. Clinically, despite their amplified ERBB2, such tumors are usually treated as HR+ luminal tumors, with 75% of PDM TPBC classified as Luminal B and 5% classified as Luminal A by PAM 50 analysis (**Supplementary Fig. S5A**).

Frontline treatments for luminal, HR+ breast cancers include a variety of estrogen blocking therapies including the selective estrogen receptor modulator, Tamoxifen. Given our observation that Stat3 inhibition reverts Mcam-KD Py230 cells to an HSP/LP transcriptional state and prior reports that inhibition of Stat3 can increase the sensitivity of multiple breast cancer cell lines to tamoxifen treatment, we next tested the sensitivity of control and Mcam-KD Py230 cells to tamoxifen using an *in vitro* proliferation assay (**Figure 5D,E**). We find that control cells are more sensitive to tamoxifen than Mcam-KD cells, and that sensitivity can be restored in Mcam-KD Py230 cells by treatment with inhibitors of Stat3 or the upstream regulator, Ck2 (**Figure 5D,E**). Together, these data further indicate that Mcam is responsible for maintaining a hormone-sensing cell state through modulation of Ck2 and downstream Stat3 signaling.

MCAM promotes tumorigenicity through cell state control.

Finally, we examined whether cell state and signaling changes observed in Mcam-KD cells *in vitro*, alter tumorigenic potential of the cells *in vivo* or whether they alter the neural crest associated, basal-like, Sox10-positive phenotype previously associated with Py230 cells *in vivo* (**Figure 5C**) (28). Surprisingly, given the apparent increase in mesenchymal traits observed when Mcam is knocked down in these cells, they were less tumorigenic than control cells in the graft setting (**Figure 6A**). Specifically, when 1,000 Py230 control or Mcam-KD cells were orthotopically transplanted into the mammary fat pads of nude mice and allowed to grow for 8-weeks, Mcam-KD-derived grafts failed to form palpable tumors, though 7 of 8 control grafts formed tumors by this time (**Figure 6A**). When 1,000,000 cells were orthotopically transplanted into the mammary fat pads, we saw formation of both control and Mcam-KD-derived tumors, but the tumors that form were fundamentally different in terms of size, histopathological appearance, and expression of select cell type markers (**Figure 6B**). Consistent with the findings of Dravis et al., we found that Py230 cells exhibit expression of Sox10 *in vivo*

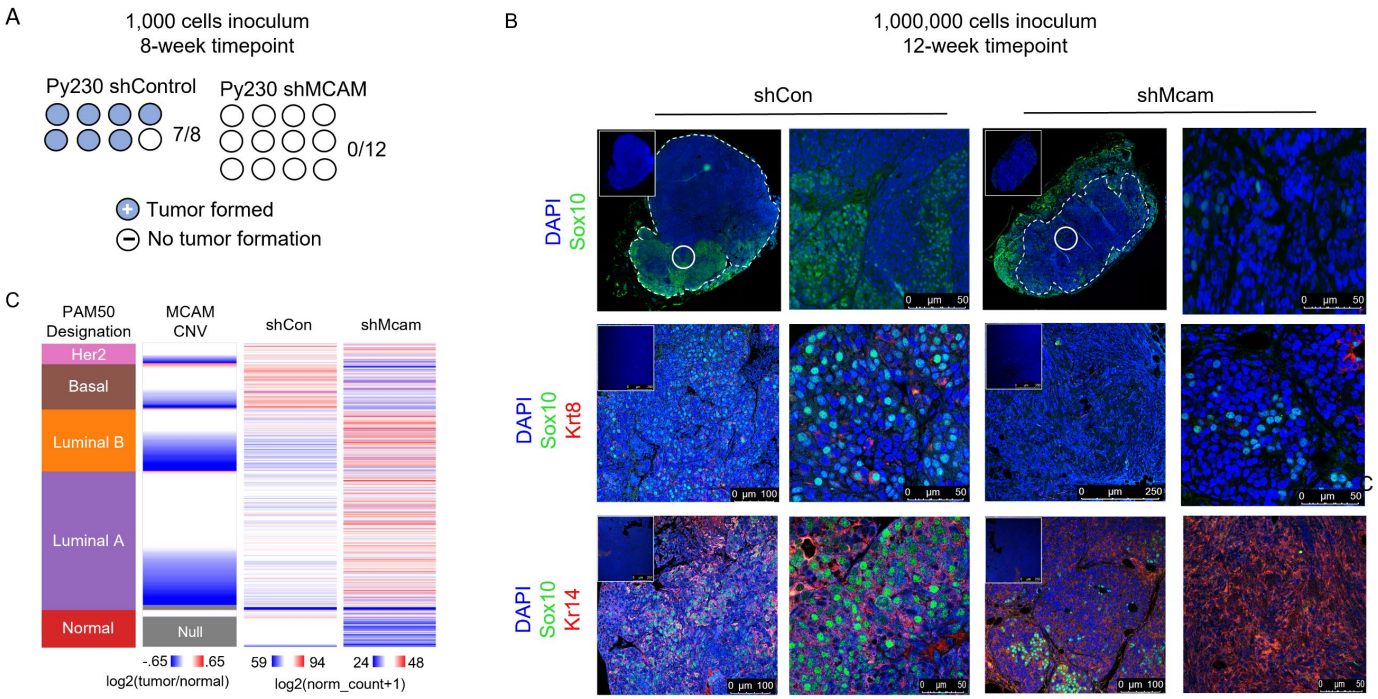

Figure 6. Mcam promotes tumorigenic phenotypes and tumor cell plasticity. A) Reduced tumor seeding capacity of Mcam-KD Py230 cells with 1,000 cell orthotopic injection after 8 weeks of growth. B) Altered cell type distribution in tumors *in vivo* generated from orthotopic injection of 10e6 Py230 control or Mcam-KD cells. IHC analysis shows differential expression and distribution of cell type markers between control and Mcam-KD tumors. Sox10+ tumor margins are demarcated from tumor parenchyma (dashed lines). Regions of interest in low magnification images marked by white circles. C) TCGA breast cancer data organized by PAM50 designation, MCAM copy number loss, and relative expression of genes with ten greatest rank changes up or down between control and shMCAM Py230 cells. Two-way ANOVA *p<.0001.*

though it is not expressed in standard tissue culture settings (**Figure 6B and data not shown**) (28). Sox10 expression *in vivo* marked large invasive peripheral regions of Py230 tumors consistent with the previously proposed neural crest like differentiation state. We determined cells in such regions co-express Krt14 suggesting these are likely basal-like regions (**Figures 5C, 6B**).

However, these large uniform Sox10+Krt14+ positive regions were wholly absent in Mcam-KD tumors and the many fewer Sox10 positive cells that were found in Mcam-KD tumors were found in organized Krt8+ epithelial structures resembling the Sox10 positive luminal cells previously described in the normal mouse mammary epithelium (**Figure 6B**) (50). Gene expression profiling of control and Mcam-KD tumors showed changes consistent with a block to the basal-like phenotype when Mcam is knocked down (**Figure 6C**).

DISCUSSION

Lineage plasticity is critical for proper mammary gland development and maintenance, however, in the context of breast cancer, lineage plasticity can drive increased tumor heterogeneity and treatment failure (7,8). Although overexpression of Mcam has previously been shown to promote EMT in mammary epithelial cells,

here we report significant Mcam expression among luminal epithelial breast cancer cell lines and the surprising finding that Mcam is required to maintain the epithelial LP-like ground state of the Py230 model, a transplantable mouse mammary cancer cell line that is typified as stem-like with a high frequency of multi-lineage keratin co-expression. Mcam KD promoted differentiation toward AVP/BP phenotypes with associated alterations in adhesion and motility and insensitivity to the selective estrogen modulator, tamoxifen, and appears to block access to hormone sensing mammary progenitor and Sox10 positive neural crest-like/ basal-like cell states.

Mechanistically, the cell state switch mediated by Mcam KD was associated with elevated paxillin and altered Src family kinase/Fak/Akt activation. The state switch was dependent on deregulated Ck2 activity leading to Stat3 activation and expression of Stat3 target genes associated with the alveolar and basal fates. Yet, we noted that Mcam effects appear to be cell type and breast cancer subtype specific as 1) expression in the basal like 4T1 cell line promotes, rather than inhibits, Stat3 activation, 2) several cell lines showed marginal to undetectable Stat3 alterations under Mcam KD and 3) Mcam expression among hormone receptor positive breast cancers was enriched among those that (like Py230) co-express ERBB2 and classify as Luminal B (**Supplementary Fig. S3A** and (39)). We propose that the cell type specificity of Mcam effects may reflect coupling or decoupling upstream kinases (such as Ck2) to different client proteins depending on a cell's ground state, i.e., luminal, basal, alveolar, Her2, etc. Indeed, Ck2 is a constitutively active high level regulatory kinase with hundreds of substrates whose mechanism of regulation and roles in mammary lineage control are not well understood, and a Ck2 binding site on the Mcam tail has been proposed but not formally tested (27).

Despite the increased mesenchymal features and therapy resistance observed for Mcam-KD Py230 cells *in vitro*, Mcam KD reduced tumorigenic seeding and growth of grafted cells in mice, a result that is at least superficially consistent with prior studies correlating Mcam expression to tumor aggressiveness (16,20,22). However, this too may be subtype dependent as re-analysis of archival TCGA breast cancer data showed Mcam expression to be a favorable marker in luminal tumors and showed Mcam loss to typify the more aggressive and more frequently tamoxifen resistant Luminal B subtype as well as the more proliferative (by gene signature) samples among Luminal A tumors.

By contrast, Mcam expressing tumors are typically Basal-like. In this regard, it is noteworthy that a recent

study suggested that Basal-like phenotypes arise from luminal progenitors and 'involution mimicry', thus invoking a critical role for LP→AVP fate switch. Based on our data and analysis of TCGA, we speculate that Mcam may be essential for the emergence of basal like tumors arising from the luminal progenitor. It should be noted that comparative transcriptomics did not indicate a strong association between Luminal B tumors in TCGA and Mcam-KD Py230. The recurrent genetic aberration at 11q that typifies most of the TCGA Breast cancers with Cyclin D amplification and Mcam copy number reduction usually involves concomitant loss of several additional 11q genes that may contribute to cell phenotype (e.g., PGR, ATM, etc.) (2,3,49) (**Supplementary Fig. S5C,D**). Thus, it is reasonable to assume that several additional genetic alterations may cooperate with Mcam loss in the context of Luminal B tumors in humans. Interestingly, altered tamoxifen responses have been associated with 11q deletions in human breast cancer although the specific genes responsible for this effect remain uncertain (49). Indeed, although the HCI-040 PDM we examined exhibits evidence of reduced Mcam expression and endocrine insensitivity it also has indications of other 11q alterations (i.e., ATM deletion) (46).

The findings above may be key to designing combination therapies that effectively manage shifting therapeutic vulnerabilities that derive from the plastic cell state change potential of mammary luminal progenitors. For instance, newer Ck2 inhibitors or Stat3 inhibitors may be of interest in combination with hormone receptor targeted therapies for some cancers (40,51). Indeed, a recent study demonstrated Stat3 inhibition can increase the tamoxifen sensitivity of tamoxifen-resistant breast cancer cells (40). Alternatively, if Mcam expression permits access to invasive neural crest like states *in vivo,* it may be more effective to inhibit MCAM and seek out new vulnerabilities of the resultant hormone insensitive cell state. Altogether, our studies indicate that Mcam plays a critical role in breast cancer cell state determination via Ck2 and Stat3 control, with implications for understanding developmental plasticity and MCAM's role in breast cancer intra- and intertumoral heterogeneity.

METHODS

Cell lines and Cell culture:

Met-1 and NDL-1 cell lines were provided by Dr. Alexander Borowsky (52,53). Authenticated 4T1 (RRID: CVCL_0125), E0771 (RRID:CVCL_GR23) cell lines were obtained from ATCC. 4T1, E0771, NDL-1, and Met-1

cells were cultured in Dulbecco's modified Eagle's media (DMEM) with ciprofloxacin 10 µg/ml and 10% fetal calf serum. Py230 cell line was kindly provided by L. Ellies (6). Identity of gifted lines is authenticated herein through molecular assays (e.g., scRNASeq,) that match profiles reported for these lines. Passage numbers were tracked and minimized, and experiments were repeated 2-8 times including repetition with early passage frozen aliquots. Py230 cells were cultured in F12-Kaighn's Modified Media with 5% fetal calf serum, ciprofloxacin 10µg/ml, amphotericin B 2.5µg/ml, and Mito+ serum extender (Corning #355006). Cells were grown in sterile humidified tissue culture incubators at 37 °C with 5% CO_2 and ambient (~ 17–18%) O_2. Cells were transduced with lentiviral concentrates in the presence of 7 µg/ml polybrene for up to 16 h with transduction efficiency (not shown) suggesting MOI <<1. CX-4945/Silmitasertib (Selleck Chem #S2248), (E/Z)-GO289 (MedChem Express, #HY-115519), Ag490 (Selleck Chem #S1143), Stattic/S7947 (S7947, Sigma Aldrich #19983-44-9), and tamoxifen citrate (Selleck Chem #S1972) were resuspended in DMSO according to manufacturers' recommendations and diluted to final concentrations in media immediately prior to being added to cells.

Lentiviral vectors:

Viral vector plasmids were obtained from OriGene Technologies, Inc. (Rockville, MD), including the mouse Mcam shRNA lentiviral plasmid (Cat # TL514377), a scrambled shControl, and a custom shRNA-resistant (via silent-mutation) mouse Mcam construct subcloned into a lentiviral gene expression vector (pLenti-C-mCFP-P2A-BSD), (# PS100107). Completed vectors were sequenced confirmed.

Western Blot:

Cell were lysed in RIPA buffer (1X PBS (137mM NaCl; 2.7mM KCl; 4.3mM Na2PO4; 1.47 mM KH2PO4) with 1% Nonidet P-40 Substitute (Sigma #74385), 0.5% Sodium deoxycholate, 0.1% SDS) with the Halt Protease & Phosphatase inhibitor cocktail (Thermo Fisher Scientific, #78440) , quantified with the RC-DC Protein Quantification Assay (BioRad) and equivalent concentrations (10-16ug) loaded per sample on precast NuPAGE 4-12% Bis-Tris gradient gels (Invitrogen). Separated proteins were transferred to nitrocellulose and probed overnight with primary antibodies under agitation. Secondary antibodies were incubated with blots for

1hr. Intervening washes used TBST pH7.5 (10mM Tris, 15mM NaCl, 0.05%Tween 20), Blots were imaged on an Odyssey CLx Imager (LI-COR).

Immunohistochemistry:

Freshly dissected tissues were fixed overnight at 4°C in 10% neutral buffered formalin (Sigma; HT501128). Fixed tissues were transferred to 70% ethanol for storage at 4 °C. Processing for histology followed standard protocols with paraffin embedding, sectioning at 5 µm thickness, baking for 1 h at 55 °C, and deparaffinizing with CitriSolv (Decon Labs, 89426-268) and rehydration through graded alcohol/water washes. Antigen retrieval was achieved by boiling samples 15min in citrate buffer (10 mM citric acid, 0.05% Tween 20, pH 6.0) prior to overnight primary antibody staining. Slides were mounted in Fluormount-G (Electron Microscopy Sciences). Slides were imaged on a Leica SP8 White light Laser Confocal microscope.

Antibodies:

Antibody	Clone	Manufacturer	Catalogue #	Assay	Dilution	RRID
anti-Akt	40D4	Cell Signaling Technology	2920	WesternBlot	1:2000	AB_1147620
anti-phospho-Akt (Ser473)	D9E	Cell Signaling Technology	4060	WesternBlot	1:2000	AB_2315049
anti-β-actin	W16197A	Biolegend	664802	WesternBlot	1:2000	AB_2721349
anti-phospho-Stat3 (Tyr705)	D3A7	Cell Signaling Technology	9145	WesternBlot	1:1000	AB_2491009
anti-Stat3	124H6	Cell Signaling Technology	9139	WesternBlot	1:1000	AB_331757
anti-Fyn	E3	Santa Cruz Biotechnology	SC-365913	WesternBlot	1:500	AB_10842309
anti-Lyn	C13F9	Cell Signaling Technology	2796T	WesternBlot	1:1000	AB_2138391
anti-phospho-src-family (Tyr418)	EP503Y	Abcam	Ab40660	WesternBlot	1:1000	AB_776106
anti-Mcam	281	Novus Biologicals	NBP2-90721	WesternBlot	1:1000	unavailable
anti-MCAM	EPR3208	Abcam	Ab75769	WesternBlot	1:1000	AB_2143375
anti-phospho-Pten (Ser380/Thr382/383)	44A7	Cell Signaling Technology	9549	WesternBlot	1:1000	AB_659891
anti-Pten	A2B1	Santa Cruz Biotechnology	SC-7974	WesternBlot	1-500	AB_628187
anti-phospho-Fak (Ty925)	polyclonal	Cell Signaling Technology	3284	WesternBlot	1:1000	AB_10831810
anti-phospho-Fak (Tyr397	D20B1	Cell Signaling Technology	8556	WesternBlot	1:1000	AB_10891442
anti-Fak	polyclonal	Cell Signaling Technology	3285	WesternBlot	1:1000	AB_2269034
anti-phospho-Stat5 (Tyr694)	D47E7	Cell Signaling Technology	4322	WesternBlot	1:400	AB_10544692
anti-Stat5	ST5-8F7	Thermo Fisher Scientific	33-5900	WesternBlot	1:200	AB_2533129
anti-Rabbit-IgG-AF680	polyclonal	Thermo Fisher Scientific	A-21076	WesternBlot	1:1000	AB_2535736
anti-Mouse-IgG-AF790	polyclonal	Thermo Fisher Scientific	A11375	WesternBlot	1:1000	AB_2534146
anti-Rat-IgG-H&LDyLight-800	polyclonal	Thermo Fisher Scientific	SA5-10032	WesternBlot	1:10000	AB_2556612
anti-Paxillin	Y113	Abcam	Ab32084	WesternBlot	1:5000	AB_779033
anti-Sox10	SD204-04	Thermo Fisher Scientific	MA5-32398	Immunocytochemistry	1:50	AB_2809676
anti-Krt14	LL002	Thermo Fisher Scientific	MA5-11599	Immunocytochemistry	1:50	AB_10982092
anti-Krt8	TROMA-1	DSHB U of Iowa	Ab-531826	Immunocytochemistry	1:50	AB_531826
anti-Rabbit-IgG-AF568	polyclonal	Thermo Fisher Scientific	A-11011	Immunocytochemistry	1:200	AB_143157
anti-Mouse-IgG-AF647	polyclonal	Thermo Fisher Scientific	A28181	Immunocytochemistry	1:200	AB_2536165
anti-Rat-IgG-AF647	polyclonal	Thermo Fisher Scientific	A-21247	Immunocytochemistry	1:200	AB_141778
anti-Mcam	ME9F1	Biolegend	313605	FACS	1:100	AB_345299
anti-CD326	G8.8	Thermo Fisher Scientific	25-5791-80	FACS	1:160	AB_1724047
anti-Sca1	D7	Thermo Fisher Scientific	17-5981-81	FACS	1:300	AB_469486
anti-Ncam1	EPR21827	Abcam	Ab220360	FACS	1:500	AB_2927664

scRNA Sequencing:

All protocols used to generate scRNA-seq data on 10x Genomics Chromium Controller platform including library prep, instrument and sequencing setting can be found on: https://www.10xgenomics.com/support/single-cell-gene-expression/documentation. The Chromium Next GEM Single Cell 3' Kit v3.1 (PN-1000268) was used to barcode individual cells with 16nt 10x Barcode, to tag cell specific transcript molecules with 12 nt Unique Molecular Identifier (UMI) and to capture poly (A) mRNA with 30 nt ploy(dT) sequence according to the manufactures. The following protocol based on 10x Genomics user guide (CG000315) was performed by High-Throughput Genomics Shared Resource at Huntsman Cancer Institute, University of Utah. Briefly, Py230 single cell suspension was isolated by trypsinization and resuspended in phosphate buffered saline with 0.04% bovine serum albumin. The cell suspension was filtered through 40-micron cell strainer. Viability and cell count were assessed on Countess 2 (Invitrogen, Carlsbad, CA). Equilibrium to targeted cell recovery of 6,000 cells along with 10x Gel Beads and reverse transcription reagents were loaded to Chromium Single Cell Chip G (PN-1000120) to form Gel-Bead-In EMulsions (GEMs), the nano-droplets. Within individual GEMs, barcoded cDNA generated from captured mRNA was synthesized by reverse transcription at the setting of 53°C for 45 min followed by 85°C for 5 min. Subsequent fragmentation, end repair and A-tailing, adaptor ligation and sample indexing with dual index (PN-1000215) were performed in bulk according to the user guide. The resulting barcoded libraries were qualified using Agilent D1000 ScreenTape on Agilent Technology 2200 TapeStation system and quantified by quantification PCR using KAPA Biosystems Library Quantification Kit for Illumine Platforms (KK4842). Multiple libraries were then normalized, pooled and sequenced on NovaSeq 6000 with 150x150 paired end mode.

Bulk RNA-sequencing:

RNA was collected from snap frozen biological replicates of 10e6 Py230 shControl/shMcam cell-derived tumors that were collected 12-weeks after inoculation. RNA was isolated via QIAzol-chloroform extraction followed by column-based purification and On-Column DNase Digestion (Qiagen #79254). The aqueous phase was brought to a final concentration of 50% ethanol, and RNA was purified using the RNeasy Lipid Tissue Mini Kit according to the manufacturer's instructions (Qiagen #74804). Library preparation was performed using the

Illumina TruSeq Stranded mRNA Library Prep with UDI (Illumina; poly(A) selection). Sequencing was performed using the NovaSeq 6000 (50 x 50 bp paired-end sequencing; 25 million reads per sample).

Bioinformatic Analysis:

All downstream analysis of sequencing data was completed using Loupe Browser (6.0.0) (RRID:SCR_018555), Enrichr (RRID:SCR_001575), Appyters (RRID:SCR_021245), GraphPad Prism (RRID:SCR_002798) and RStudio (4.1.2) (RRID:SCR_000432). For differential gene expression analysis, we utilized the default clustering method of Seurat with the Louvain algorithm to iteratively group cells together (54). Reanalysis of primary mouse mammary data from Giraddi et al. used the published diffusion map coordinates and the markers Krt14, Krt8 and Wfdc18, to designate 4 adult groups/cell-types, basal, luminal differentiated, luminal progenitor, and alveolar (15). We used the Seurat default differential expressed gene (DEG) test [FindMarkers()] (non-parametric Wilcoxon rank sum test). The top 100 DEGs were then used for downstream comparative analysis. From the Py230 dataset, DEG lists were generated by comparing the shCon luminal to shMcam luminal clusters and similarly for the alveolar clusters identified through marker gene comparisons. We used GSEA software (RRID:SCR_005724), and Molecular Signature Database (MSigDB; RRID:SCR_016863) (33) to compare gene sets with 100,000 permutations in GSEA Pre-ranked. GSEA data was plotted with GraphPad Prism (RRID:SCR_002798). Kaplan Meier plots were generated using TCGA data visualized utilizing KMplot and the auto-select cutoff values for Basal (3.45), Luminal A (3.35), Luminal B (3.29) and Her2 (2.97). (55). Heatmaps and MCAM CNV analysis utilized the UCSC Xena Browser (48) (RRID:SCR_018938).

Tumor studies:

10-week-old nude female mice were from Charles River Laboratories (Wilmington, MA). 1,000 or 1,000,000 MMTV-PyMT Py230 cells were resuspended in complete Matrigel (Corning) and orthotopically injected into the #4 mammary glands of mice. At endpoint, mice were euthanized according to AVMA guidelines and tissues were harvested for processing.

Statistics:

Replicates and experimental repetition are indicated in figures and figure legends**.** For statistical analysis, One-Way ANOVA with Tukey Kramer Multiple Comparisons, Repeated Measures One-Way ANOVA (Geisser-Greenhouse correction) w/ Tukey multiple comparison tests, and Two-Way ANOVA with Sidak's multiple comparisons were used. ** p<0.05, ** p<0.01, *** p<0.001, **** p<0.0001.* Gene mapping and differential gene expression analysis utilized established default methods embedded in the Cell Ranger, CLoupe browser and Seurat computational packages.

Study Approval:

All animal care and procedures were approved and monitored by an Institutional Animal Care and Use Committee.

Data Availability:

The sequence data generated in this study will be made publicly available in Gene Expression Omnibus (GEO) (in progress), and within the article and its supplementary data files.

Acknowledgements:

We thank C. Trejo for technical assistance and M. Kruithof-de Julio, T. Oliver, and D. Salomon for valuable discussions. We thank the Univ. of Utah/HCI Cancer Center Support Grant (P30 CA42014), and staff in the Flow cytometry, Microscopy, Preclinical research resource, Biostatistics, High-throughput Genomics and Bioinformatics shared core resources. We also acknowledge generous support from the Huntsman Cancer Foundation, and from the Halt Cancer at X foundation.

Contributions:

Concept: BTS. Experimental Design: OB, BLG, BTS. Execution: OB, BLG, DWF, BH, BTS. Analysis: BLG, EMM, DA-T. Interpretation: All authors. Writing: OB, BLG, BTS.

REFERENCES

1. Testa U, Castelli G, Pelosi E. Breast Cancer: A Molecularly Heterogenous Disease Needing Subtype-Specific Treatments. Med Sci (Basel) **2020**;8
2. Sorlie T, Perou CM, Tibshirani R, Aas T, Geisler S, Johnsen H*, et al.* Gene expression patterns of breast carcinomas distinguish tumor subclasses with clinical implications. Proc Natl Acad Sci U S A **2001**;98:10869-74
3. Ades F, Zardavas D, Bozovic-Spasojevic I, Pugliano L, Fumagalli D, de Azambuja E*, et al.* Luminal B breast cancer: molecular characterization, clinical management, and future perspectives. J Clin Oncol **2014**;32:2794-803
4. Kensler KH, Sankar VN, Wang J, Zhang X, Rubadue CA, Baker GM*, et al.* PAM50 Molecular Intrinsic Subtypes in the Nurses' Health Study Cohorts. Cancer Epidemiol Biomarkers Prev **2019**;28:798-806
5. Smith BA, Shelton DN, Kieffer C, Milash B, Usary J, Perou CM*, et al.* Targeting the PyMT Oncogene to Diverse Mammary Cell Populations Enhances Tumor Heterogeneity and Generates Rare Breast Cancer Subtypes. Genes Cancer **2012**;3:550-63
6. Bao L, Cardiff RD, Steinbach P, Messer KS, Ellies LG. Multipotent luminal mammary cancer stem cells model tumor heterogeneity. Breast Cancer Res **2015**;17:137
7. Wahl GM, Spike BT. Cell state plasticity, stem cells, EMT, and the generation of intra-tumoral heterogeneity. NPJ Breast Cancer **2017**;3:14
8. Kong D, Hughes CJ, Ford HL. Cellular Plasticity in Breast Cancer Progression and Therapy. Front Mol Biosci **2020**;7:72
9. Stefanovic S, Wirtz R, Deutsch TM, Hartkopf A, Sinn P, Varga Z*, et al.* Tumor biomarker conversion between primary and metastatic breast cancer: mRNA assessment and its concordance with immunohistochemistry. Oncotarget **2017**;8:51416-28
10. Zhang Y, Weinberg RA. Epithelial-to-mesenchymal transition in cancer: complexity and opportunities. Front Med **2018**;12:361-73
11. Garcia-Recio S, Hinoue T, Wheeler GL, Kelly BJ, Garrido-Castro AC, Pascual T*, et al.* Multiomics in primary and metastatic breast tumors from the AURORA US network finds microenvironment and epigenetic drivers of metastasis. Nat Cancer **2023**;4:128-47
12. Chakrabarti R, Wei Y, Romano RA, DeCoste C, Kang Y, Sinha S. Elf5 regulates mammary gland stem/progenitor cell fate by influencing notch signaling. Stem Cells **2012**;30:1496-508
13. Haricharan S, Li Y. STAT signaling in mammary gland differentiation, cell survival and tumorigenesis. Mol Cell Endocrinol **2014**;382:560-9
14. Caffarel MM, Zaragoza R, Pensa S, Li J, Green AR, Watson CJ. Constitutive activation of JAK2 in mammary epithelium elevates Stat5 signalling, promotes alveologenesis and resistance to cell death, and contributes to tumourigenesis. Cell Death Differ **2012**;19:511-22
15. Giraddi RR, Chung CY, Heinz RE, Balcioglu O, Novotny M, Trejo CL*, et al.* Single-Cell Transcriptomes Distinguish Stem Cell State Changes and Lineage Specification Programs in Early Mammary Gland Development. Cell Rep **2018**;24:1653-66 e7
16. Wang Z, Xu Q, Zhang N, Du X, Xu G, Yan X. CD146, from a melanoma cell adhesion molecule to a signaling receptor. Signal Transduct Target Ther **2020**;5:148
17. Pal B, Chen Y, Vaillant F, Jamieson P, Gordon L, Rios AC*, et al.* Construction of developmental lineage relationships in the mouse mammary gland by single-cell RNA profiling. Nat Commun **2017**;8:1627
18. Spike BT, Engle DD, Lin JC, Cheung SK, La J, Wahl GM. A mammary stem cell population identified and characterized in late embryogenesis reveals similarities to human breast cancer. Cell Stem Cell **2012**;10:183-97

19. Imbert AM, Garulli C, Choquet E, Koubi M, Aurrand-Lions M, Chabannon C. CD146 expression in human breast cancer cell lines induces phenotypic and functional changes observed in Epithelial to Mesenchymal Transition. PLoS One **2012**;7:e43752
20. Liang YK, Zeng D, Xiao YS, Wu Y, Ouyang YX, Chen M*, et al.* MCAM/CD146 promotes tamoxifen resistance in breast cancer cells through induction of epithelial-mesenchymal transition, decreased ERalpha expression and AKT activation. Cancer Lett **2017**;386:65-76
21. Huang CY, Wu GJ. METCAM/MUC18 promoted tumorigenesis of human breast cancer SK-BR-3 cells in a dosage-specific manner. Taiwan J Obstet Gynecol **2016**;55:202-12
22. Zabouo G, Imbert AM, Jacquemier J, Finetti P, Moreau T, Esterni B*, et al.* CD146 expression is associated with a poor prognosis in human breast tumors and with enhanced motility in breast cancer cell lines. Breast Cancer Res **2009**;11:R1
23. Leroyer AS, Blin MG, Bachelier R, Bardin N, Blot-Chabaud M, Dignat-George F. CD146 (Cluster of Differentiation 146). Arterioscler Thromb Vasc Biol **2019**;39:1026-33
24. Ruma IM, Putranto EW, Kondo E, Murata H, Watanabe M, Huang P*, et al.* MCAM, as a novel receptor for S100A8/A9, mediates progression of malignant melanoma through prominent activation of NF-kappaB and ROS formation upon ligand binding. Clin Exp Metastasis **2016**;33:609-27
25. Ishikawa T, Wondimu Z, Oikawa Y, Gentilcore G, Kiessling R, Egyhazi Brage S*, et al.* Laminins 411 and 421 differentially promote tumor cell migration via alpha6beta1 integrin and MCAM (CD146). Matrix Biol **2014**;38:69-83
26. Ye Z, Zhang C, Tu T, Sun M, Liu D, Lu D*, et al.* Wnt5a uses CD146 as a receptor to regulate cell motility and convergent extension. Nat Commun **2013**;4:2803
27. Wu G-J. METCAM/MUC18 expression and cancer metastasis. Current Genomics **2005**;6:333-49
28. Dravis C, Chung CY, Lytle NK, Herrera-Valdez J, Luna G, Trejo CL*, et al.* Epigenetic and Transcriptomic Profiling of Mammary Gland Development and Tumor Models Disclose Regulators of Cell State Plasticity. Cancer Cell **2018**;34:466-82 e6
29. Sorrentino A, Ferracin M, Castelli G, Biffoni M, Tomaselli G, Baiocchi M*, et al.* Isolation and characterization of CD146+ multipotent mesenchymal stromal cells. Exp Hematol **2008**;36:1035-46
30. Webb DJ, Donais K, Whitmore LA, Thomas SM, Turner CE, Parsons JT*, et al.* FAK-Src signalling through paxillin, ERK and MLCK regulates adhesion disassembly. Nat Cell Biol **2004**;6:154-61
31. Shehata M, Teschendorff A, Sharp G, Novcic N, Russell IA, Avril S*, et al.* Phenotypic and functional characterisation of the luminal cell hierarchy of the mammary gland. Breast Cancer Res **2012**;14:R134
32. Bach K, Pensa S, Grzelak M, Hadfield J, Adams DJ, Marioni JC*, et al.* Differentiation dynamics of mammary epithelial cells revealed by single-cell RNA sequencing. Nat Commun **2017**;8:2128
33. Subramanian A, Tamayo P, Mootha VK, Mukherjee S, Ebert BL, Gillette MA*, et al.* Gene set enrichment analysis: a knowledge-based approach for interpreting genome-wide expression profiles. Proc Natl Acad Sci U S A **2005**;102:15545-50
34. Xie Z, Bailey A, Kuleshov MV, Clarke DJB, Evangelista JE, Jenkins SL*, et al.* Gene Set Knowledge Discovery with Enrichr. Curr Protoc **2021**;1:e90
35. De Vos J, Jourdan M, Tarte K, Jasmin C, Klein B. JAK2 tyrosine kinase inhibitor tyrphostin AG490 downregulates the mitogen-activated protein kinase (MAPK) and signal transducer and activator of transcription (STAT) pathways and induces apoptosis in myeloma cells. Br J Haematol **2000**;109:823-8
36. Yeo SK, Zhu X, Okamoto T, Hao M, Wang C, Lu P*, et al.* Single-cell RNA-sequencing reveals distinct patterns of cell state heterogeneity in mouse models of breast cancer. Elife **2020**;9
37. Tai CI, Schulze EN, Ying QL. Stat3 signaling regulates embryonic stem cell fate in a dose-dependent manner. Biol Open **2014**;3:958-65
38. Chapman RS, Lourenco PC, Tonner E, Flint DJ, Selbert S, Takeda K*, et al.* Suppression of epithelial apoptosis and delayed mammary gland involution in mice with a conditional knockout of Stat3. Genes Dev **1999**;13:2604-16

39. Hughes K, Watson CJ. The Multifaceted Role of STAT3 in Mammary Gland Involution and Breast Cancer. Int J Mol Sci **2018**;19
40. Moon SY, Lee H, Kim S, Hong JH, Chun SH, Lee HY*, et al.* Inhibition of STAT3 enhances sensitivity to tamoxifen in tamoxifen-resistant breast cancer cells. BMC Cancer **2021**;21:931
41. Schust J, Sperl B, Hollis A, Mayer TU, Berg T. Stattic: a small-molecule inhibitor of STAT3 activation and dimerization. Chem Biol **2006**;13:1235-42
42. Zheng Y, Qin H, Frank SJ, Deng L, Litchfield DW, Tefferi A*, et al.* A CK2-dependent mechanism for activation of the JAK-STAT signaling pathway. Blood **2011**;118:156-66
43. Filhol O, Deshiere A, Cochet C. Role of CK2 in the Control of Cell Plasticity in Breast Carcinoma Progression. Protein Kinase CK22013. p 363-82.
44. Zou J, Luo H, Zeng Q, Dong Z, Wu D, Liu L. Protein kinase CK2alpha is overexpressed in colorectal cancer and modulates cell proliferation and invasion via regulating EMT-related genes. J Transl Med **2011**;9:97
45. Miller SJ, Lou DY, Seldin DC, Lane WS, Neel BG. Direct identification of PTEN phosphorylation sites. FEBS Lett **2002**;528:145-53
46. Guillen KP, Fujita M, Butterfield AJ, Scherer SD, Bailey MH, Chu Z*, et al.* A human breast cancer-derived xenograft and organoid platform for drug discovery and precision oncology. Nat Cancer **2022**;3:232-50
47. Cancer Genome Atlas N. Comprehensive molecular portraits of human breast tumours. Nature **2012**;490:61-70
48. Goldman MJ, Craft B, Hastie M, Repecka K, McDade F, Kamath A*, et al.* Visualizing and interpreting cancer genomics data via the Xena platform. Nat Biotechnol **2020**;38:675-8
49. Lundgren K, Holm K, Nordenskjold B, Borg A, Landberg G. Gene products of chromosome 11q and their association with CCND1 gene amplification and tamoxifen resistance in premenopausal breast cancer. Breast Cancer Res **2008**;10:R81
50. Dravis C, Spike BT, Harrell JC, Johns C, Trejo CL, Southard-Smith EM*, et al.* Sox10 Regulates Stem/Progenitor and Mesenchymal Cell States in Mammary Epithelial Cells. Cell Rep **2015**;12:2035-48
51. Chua MM, Ortega CE, Sheikh A, Lee M, Abdul-Rassoul H, Hartshorn KL*, et al.* CK2 in Cancer: Cellular and Biochemical Mechanisms and Potential Therapeutic Target. Pharmaceuticals (Basel) **2017**;10
52. Borowsky AD, Namba R, Young LJ, Hunter KW, Hodgson JG, Tepper CG*, et al.* Syngeneic mouse mammary carcinoma cell lines: two closely related cell lines with divergent metastatic behavior. Clin Exp Metastasis **2005**;22:47-59
53. Siegel PM, Ryan ED, Cardiff RD, Muller WJ. Elevated expression of activated forms of Neu/ErbB-2 and ErbB-3 are involved in the induction of mammary tumors in transgenic mice: implications for human breast cancer. EMBO J **1999**;18:2149-64
54. Hao Y, Hao S, Andersen-Nissen E, Mauck WM, 3rd, Zheng S, Butler A*, et al.* Integrated analysis of multimodal single-cell data. Cell **2021**;184:3573-87 e29
55. Lanczky A, Gyorffy B. Web-Based Survival Analysis Tool Tailored for Medical Research (KMplot): Development and Implementation. J Med Internet Res **2021**;23:e27633